Indoor Environmental Quality Monitoring by Autonomous Mobile Sensing

Ming Jin
UC Berkeley

Shichao Liu
UC Berkeley

Yulun Tian
UC Berkeley

Mingjian Lu
UC Berkeley

Stefano Schiavon
UC Berkeley

Costas Spanos
UC Berkeley

ABSTRACT

Indoor environmental quality (IEQ) monitoring is a critical task in building operation, maintenance, and diagnosis. Current approach based on static sensor network is not scalable for IEQ assessment that relies on costly sensing instruments. The study proposes to leverage *autonomous mobility* to reduce sensing infrastructure cost and enable real-time high-granularity monitoring that can be otherwise inhibitively laborious. Unique to the autonomous mobile sensing methodology, the collected IEQ samples are highly sparse in both spatial and temporal domains. The study develops spatio-temporal (ST) interpolation methods based on ST binning, global trend extraction, and local variation estimation, which efficiently use the data to construct accurate depiction of the indoor environment evolution. The method is evaluated by a standard protocol for ventilation assessment, where the estimation is shown to be highly correlated with the ground truth, and reveals the true ventilation conditions.

CCS CONCEPTS

• **Information systems → Sensor networks**; • **Human-centered computing → Mobile computing**;

KEYWORDS

Indoor environmental quality, mobile sensing, spatio-temporal interpolation

1 INTRODUCTION

Buildings are among the most important cyber-physical energy systems, accounting for 40% of the primary energy usage and 74% of the electrical energy in the U.S.[1]. With the convergence and mutual strengthening of internet-of-things (IoT) and information technology, buildings can provide ancillary service to the grid and attend to occupancy comfort, productivity, and health [2–5]. Indoor climate monitoring is crucial for building agility, enabling indoor environmental quality (IEQ) assessment [3], occupancy-based climate control [6–8], and context-aware services [9]. While instrumenting the space with low-cost sensors like temperature, humidity, and light level, is a viable option, it is not scalable for expensive sensors like carbon dioxide (CO_2), ozone, particulate matters (in particular $PM_{2.5}$), volatile organic compounds (VOC), sound pressure level, which are standard parameters in IEQ assessment [4, 10]. Previously, these instruments are placed on a cart manually navigated throughout the space to take measurements, which can be inhibitively laborious [4].

To enable real-time scalable indoor monitoring, the study proposes to leverage autonomous sensing using a navigation-capable robot, where vairous indoor positioning techniques based on vision, iBeacon, and WiFi can be leveraged for the self-positioning [11–13]. The key challenge is the utilization of spatially and temporally sparse samples to reconstruct the field, or a problem of spatio-temporal (ST) interpolation [14, 15]. While previous works studied methods based on Kriging [14], Markov random field [15], Gaussian process [16, 17], shape functions [18], and Kalman filter [19], the data were assumed to come from multiple sensor stations and continuous in time at a given location.

Differentiated from prior arts, key contributions of the study are:

- Development of a rapid, accurate, scalable indoor monitoring system based on an autonomous mobile robot (Fig. 1);
- Proposal of spatio-temporal interpolation algorithms to explore highly sparse mobile sensing data (Fig. 2);
- Evaluation of the accuracy and reliability of the system in a case study of indoor air change effectiveness (Fig. 3).

The rest of the paper is organized as follows. The autonomous mobile sensing system, including the environmental sensing platform and the mobile robot, is introduced in Section 2. Section 3 discusses the proposed spatio-temporal method and its relation to prior arts. An application in IEQ assessment is investigated in Section 4, followed by concluding remarks in Section 5.

2 AUTONOMOUS MOBILE SENSING SYSTEM

In this section, we will introduce the environmental sensing platform (ESP) and the robotic base as the essential components in the autonomous sensing system (Fig. 1).

2.1 Environmental sensing platform (ESP)

A comprehensive list of sensors are integrated in ESP to monitor the indoor environment, including temperature and humidity, light level, PM2.5, carbon dioxide (CO_2), and organic volatile compound (VOC) (Table 1 and Fig. 1). Data are sampled and uploaded to our server using WiFi communication link at an interval of 10 s, which are pushed to the front-end visualization portal (Fig. 1).

BuildSys '17, November 8–9, 2017, Delft, Netherlands

ACM ISBN 978-1-4503-5544-5/17/11…$15.00
https://doi.org/10.1145/3137133.3137158

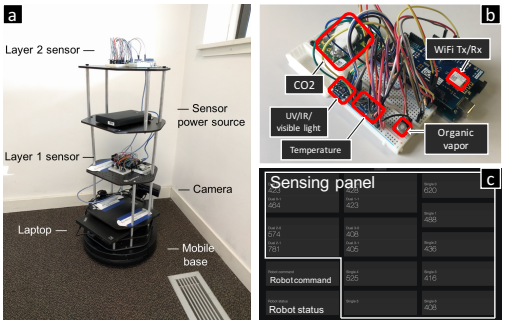

Figure 1: Snapshots of (a) the robotic platform, (b) environmental sensing platform, and (c) web-based visualization portal.

Table 1: Sensing modules of ESP.

Environmental parameter	Module	Performance	Price
Temperature	MCP9808	Accuracy: 0.25°C typical precision over -40°C to 125°C range	$4.68
UV index / IR / visible light	SI1145	Ambient light sensor: 100 mlx resolution	$9.95
CO_2	K-30	Measurement Range: 0 – 10000 ppm Accuracy: ± 3 % of measurement	$85
PM2.5	SEN0177	Measuring pm range: 0~500 $\mu g/m^3$	$46.90
Organic volatile compound	TGS2620	Typical detection range: 50 - 5000 ppm Sensitivity: 0.3~0.5 in ethano	$8.90

Based on the Arduino microcontroller board, ESP is designed on a software-level to work instantly with power-plug to relieve laborious configuration or setup, and to detect and report sensor faults automatically to alert users. In addition, sensors are calibrated using automatic baseline correction (ABC) before use.

2.2 Mobile autonomous robot

Mounted with ESP, the mobile robot (Turtlebot 2) can be controlled remotely or make decisions based on real-time sensing data (Fig. 1). Programmed under the robot operating system (ROS), it runs mapping, positioning, and navigation algorithms autonomously.

Based on the depth image from Kinect camera, the Simultaneous Localization and Mapping (SLAM) problem is solved with particle filter by tracking the robot position relative to the surroundings [12]. This enables agile operation in new and dynamic environment. Given a set of goal points, the robot is navigated using a *global planner* to set the path and a *local planner* to avoid obstacles, such as occupants and furniture.

3 SPATIO-TEMPORAL METHODS

A data-driven approach to spatio-temporal (ST) interpolation is adopted based on statistical decision theory. In particular, for indoor environment, the variation exhibits both a *global trend*, as dominated by outdoor weather, indoor emissions and HVAC operation, as well as a *local trend*, as influenced by occupants, inhomogeneous air turbulence, and furniture.

The proposed algorithm, therefore, has three key steps (Fig. 2):

(1) ST binning: consider a 4D-space (xyz and t axes represent space and time, respectively) divided into 4D cubes based on spatial and temporal resolutions. Data points are binned and aggregated to reduce measurement errors.
(2) Global trend estimation: a regression trend is fitted by, e.g., locally weighted scatterplot smoothing (LOWESS) [20], to capture the global variation.
(3) Local variation interpolation: based on the residues from global trend, a local variation function is approximated and applied on unknown points.

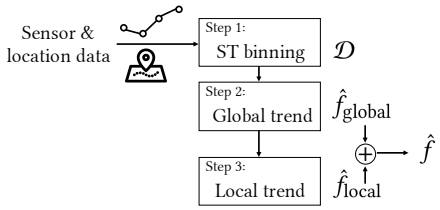

Figure 2: Illustration of ST interpolation method.

3.1 ST interpolation

Given the ST-binned dataset $\mathcal{D} = \{(s_1, t_1, v_1), ..., (s_n, t_n, v_n)\}$, where $s_i = (x_i, y_i, z_i)$ and t_i are the spatial coordinate and timestamp, and v_i is the actual value, our goal is to find a ST function, $\hat{f} : \mathbb{R}^3 \times \mathbb{R} \mapsto \mathbb{R}$, which estimates values at points of interests:

$$\hat{f}(s, t) = \hat{f}_{\text{global}}(s, t) + \hat{f}_{\text{local}}(s, t). \quad (1)$$

The first part, $\hat{f}_{\text{global}}(s, t)$, is given by the global trend estimation using LOWESS [20]. Based on the residuals $r_i = v_i - \hat{f}_{\text{global}}(s_i, t_i)$, the local variation is given by *empirical risk minimization (ERM)*:

$$\hat{f}_{\text{local}} = \arg\min_{f \in \mathcal{F}} \frac{1}{n} \sum_{i=1}^{n} l(f(s_i, t_i), r_i) \quad (2)$$

where $\mathcal{F}$ delineates the range of estimators, e.g., the class of linear regressors, and $l : \mathbb{R} \times \mathbb{R} \to \mathbb{R}$ is the loss function, which penalizes error in estimation, e.g., the squared loss $l(a, b) = (a-b)^2$. Implicitly, we assume that points close in space and time are also close in values, which is generally true for indoor environment.

A variety of algorithms to capture local variation have been implemented in our open toolset, such as K-nearest neighbor (KNN), Lasso, support vector regression (SVR), adaptive boosting (AdaBoost), random forest, and extra trees [20], which are trained by ERM with different loss functions.

3.2 Discussion

Spatial interpolation is a well-studied topic in geostatistical analysis and image processing communities, where methods like Kriging and Markov random field (MRF) are among the most prominent [14, 15]. Kriging has also been combined with Gaussian MRF [21] and principle component analysis [22] to improve the computational efficiency. Recently, Dearmon and Smith [16] augmented Gaussian process regression with Bayesian model averaging that also allows for the identification of statistically relevant explanatory variables.

While MRF is preferred for high-density data, Kriging is superior under sparse measurement, thus has been generalized to ST interpolation [14]. Shape functions were introduced by Li and Revesz [18] which are finite element methods by mesh generation. Kardia et al. also extends Kriging with Kalman filter for ST interpolation [19]. Variational Gaussian-process factor analysis is proposed by Luttinen and Ilin to model ST data [17].

Prior works assume multiple time series data from individual sensor stations; but the data from mobile sensing robot poses the challenge of high sparsity and non-continuity in time and space. The ST interpolation function (1) discerns global from local variations to efficiently capture the ST dependency with limited data.

4 APPLICATION: IEQ MAPPING

To demonstrate the effectiveness in monitoring the indoor environment, we conduct an experiment to examine the *age of air*, which is a measure of air change effectiveness and consequentially of IEQ [23].

Designed to resemble an office environment, the climate chamber (measures 5.5 × 5.5 × 2.5 m), or the experiment venue, is located at the Center for the Built Environment (CBE) at UC Berkeley. A dedicated underfloor air distribution (UFAD) system controls indoor air temperature and relative humidity at an accuracy of ± 0.5 °C and ± 3%, respectively [23]. Air was supplied from the floor and get exhausted at the ceiling level. The total supply airflow rate for all the experiment cases was approximately 79 ± 11 m^3/hr.

The robot was designated to survey 10 points covering the chamber, where ESPs are located to collect data as the ground truth. With a rover speed of about 2 m/s and a lingering time of 45 s at each survey point, it takes about 8 min to finish one round.

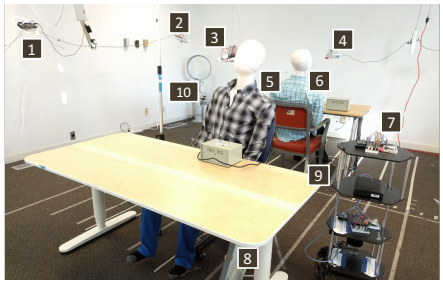

Figure 3: Testbed snapshot, showing the static sensor stations (1–4), thermal manikins to model realistic heat sources (5,6), robot (7), floor heaters (8,9), and CO_2 source (10).

To conduct the experiment, beverage-grade CO_2 is first injected into the space until the indoor concentration is uniform at about 3000 ppm. We applied one ceiling and one standing fan to well mix the indoor CO_2 and turned them off after the injection. When the airflow pattern was reestablished, ESPs took measurements of CO_2 concentration. Three conditions are considered, regarding the on/off of vents and heaters (Table 2).

By relating the locations to CO_2 measurements taken by the robot ESP, the spiral-like trace reflects the spatio-temporal evolution of CO_2 concentration (Fig. 4). While the samples are sparse in both space and time, they are accurate "snapshots" of local environment (Fig. 5), which can be used to train our ST algorithm.

Table 2: Experimental conditions for vents and heater status.

Experiment i.d.	Exp A	Exp B	Exp C
Number of open vents	1	2	2
Floor heater status	On	Off	On

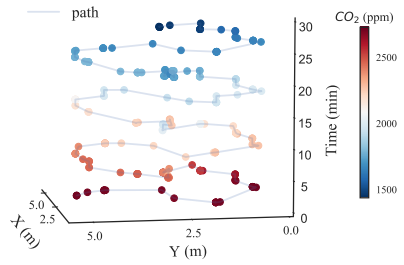

Figure 4: Trace of mobile measurements.

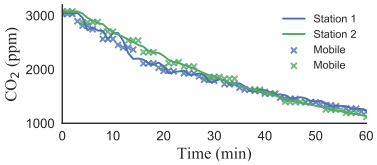

Figure 5: Collocation of mobile (x) and static (line) samples.

Let $v(t, \boldsymbol{s})$ be the added CO_2 concentration (i.e., indoor sample minus 400 ppm, the outdoor concentration) at location $\boldsymbol{s}$ and time t from the start t_{start} to finish t_{end}. The air age at $\boldsymbol{s}$ is given by [23]:

$$\tau(\boldsymbol{s}) = (t_{\text{end}} - t_{\text{start}}) \frac{v_{\text{avg}}(\boldsymbol{s})}{v(t_{\text{start}}, \boldsymbol{s})} \tag{3}$$

where $v_{\text{avg}}(\boldsymbol{s}) = \int_{t_{\text{start}}}^{t_{\text{end}}} v(t, \boldsymbol{s}) dt / (t_{\text{end}} - t_{\text{start}})$ can be estimated from ST interpolated samples.

Using only the robot ESP samples, in tandem with the proposed ST algorithms, the estimated air age is very close to the ground truth measured by ESP stationed at the location (Fig. 6). Further verification in terms of root mean squared error (RMSE) (Fig. 7 for individual experiment and Table 3 for the average across all conditions) and Pearson correlation coefficient (Fig. 8) indicates that KNN and Extra Trees are among the best estimators, outperforming significantly the baseline that disregards the location information (i.e., taking the average of all samples collected by robot ESP as $v_{\text{avg}}(\boldsymbol{s})$ without ST interpolation).

Furthermore, the spatially-differentiated air age estimation reveals critical characteristics of air change effectiveness (Fig. 9): while the air is "fresher" near the vents (one is near x: 0.5m, y: 4m, and the other: x: 1.5m, y: 5m), floor heaters are helpful to enhance thermal stratification and create a displacement airflow pattern, which improves air change effectiveness. This is important to ensure occupant comfort and health with sufficient indoor ventilation.

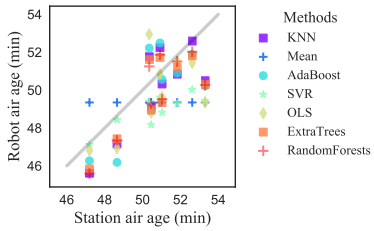

Figure 6: Plot of air age estimation by static stations and mobile robot with different local variation methods in Exp A.

Table 3: Performance of ST methods for air age estimation.

	Mean	SVR	OLS	Ridge	KNN	Rand. Forest	Extra Trees
RMSE (min)	2.07	1.69	1.40	1.40	1.26	1.31	**1.24**
Correlation	0	0.69	0.62	0.62	0.73	0.66	**0.75**

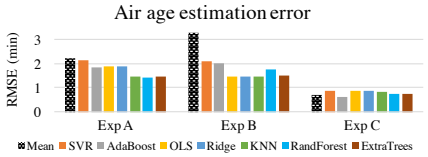

Figure 7: Air age estimation RMSE for different methods.

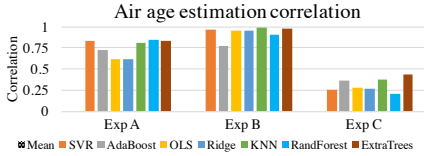

Figure 8: Pearson correlation of air age estimation.

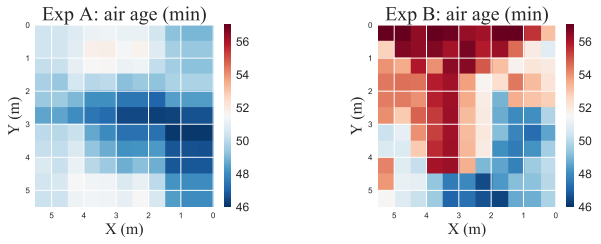

Figure 9: Comparison of spatial distributions of air age estimation in Exp A and B (see Table 2).

5 CONCLUSION

The central idea proposed in the study is to leverage *autonomous mobility* to reduce the sensing infrastructure cost to serve building operation, maintenance, and diagnosis. This can be achieved by equipping navigation-enabled robots with environmental sensing capability that can cover a large area within a building autonomously. Critical to the task is utilization of spatially and temporally sparse data collected from the mobile robot to generate continuous depiction of the environment. To this end, we propose an ST interpolation method based on ST binning, and hierarchical estimation of global and local trends. A use case of air change effectiveness is described, where autonomous mobile sensing is able to distinguish spatial patterns of air age from different ventilation settings. This information is useful to improve IEQ and energy efficiency, and importantly, occupant health, well-being and comfort.

REFERENCES

[1] S. Iyengar, S. Lee, D. Irwin, and P. Shenoy. Analyzing energy usage on a city-scale using utility smart meters. In *ACM International Conference on Systems for Energy-Efficient Built Environments*, pages 51–60, 2016.

[2] M. Jin, W. Feng, P. Liu, C. Marnay, and C. Spanos. MOD-DR: Microgrid optimal dispatch with demand response. *Applied Energy*, 187:758–776, 2017.

[3] M. Frontczak, S. Schiavon, J. Goins, E. Arens, H. Zhang, and P. Wargocki. Quantitative relationships between occupant satisfaction and satisfaction aspects of indoor environmental quality and building design. *Indoor air*, 22(2):119–131, 2012.

[4] D. Heinzerling, S. Schiavon, T. Webster, and E. Arens. Indoor environmental quality assessment models: A literature review and a proposed weighting and classification scheme. *Building and environment*, 70:210–222, 2013.

[5] M. Jin, R. Jia, and C. Spanos. Virtual occupancy sensing: Using smart meters to indicate your presence. *IEEE Transactions on Mobile Computing*, PP(99):1–14, 2017.

[6] R. Jia, R. Dong, S. Sastry, and C. Spanos. Privacy-enhanced architecture for occupancy-based hvac control. In *Proceedings of the 8th International Conference on Cyber-Physical Systems*, pages 177–186, 2017.

[7] M. Jin, N. Bekiaris-Liberis, K. Weekly, C. Spanos, and A. Bayen. Occupancy detection via environmental sensing. *IEEE Transaction on Automation Science Engineering*, (99):1–13, 2016.

[8] O. Ardakanian, A. Bhattacharya, and D. Culler. Non-intrusive techniques for establishing occupancy related energy savings in commercial buildings. In *ACM International Conference on Systems for Energy-Efficient Built Environments*, pages 21–30, 2016.

[9] N. Klingensmith, A. Sridhar, Z. LaVallee, and S. Banerjee. Spock: A sensor value prediction and online control algorithm for building resource management. In *ACM International Conference on Systems for Energy-Efficient Built Environments*, pages 123–132, 2016.

[10] J. Spengler, J. Samet, J. McCarthy, et al. *Indoor air quality handbook*. McGraw-Hill New York, 2001.

[11] H. Zou, Y. Zhou, H. Jiang, B. Huang, L. Xie, and C. Spanos. Adaptive localization in dynamic indoor environments by transfer kernel learning. In *Wireless Communications and Networking Conference (WCNC), 2017 IEEE*, pages 1–6. IEEE, 2017.

[12] D. Fox, W. Burgard, F. Dellaert, and S. Thrun. Monte carlo localization: Efficient position estimation for mobile robots. *AAAI*, pages 343–349, 1999.

[13] R. Jia, M. Jin, Z. Chen, and C. J. Spanos. Soundloc: Accurate room-level indoor localization using acoustic signatures. In *IEEE International Conference on Automation Science and Engineering*, pages 186–193, 2015.

[14] N. Cressie and C. Wikle. *Statistics for spatio-temporal data*. John Wiley & Sons, 2015.

[15] Stuart Geman and Donald Geman. Stochastic relaxation, gibbs distributions, and the bayesian restoration of images. *IEEE Transactions on pattern analysis and machine intelligence*, (6):721–741, 1984.

[16] J. Dearmon and T. Smith. Gaussian process regression and bayesian model averaging: An alternative approach to modeling spatial phenomena. *Geographical Analysis*, 48(1):82–111, 2016.

[17] Jaakko Luttinen and Alexander Ilin. Variational gaussian-process factor analysis for modeling spatio-temporal data. In *Advances in neural information processing systems*, pages 1177–1185, 2009.

[18] L. Li and P. Revesz. Interpolation methods for spatio-temporal geographic data. *Computers, Environment and Urban Systems*, 28(3):201–227, 2004.

[19] K. V Mardia, C. Goodall, E. Redfern, and F. Alonso. The kriged kalman filter. *Test*, 7(2):217–282, 1998.

[20] J. Friedman, T. Hastie, and R. Tibshirani. *The elements of statistical learning*, volume 1. Springer series in statistics Springer, Berlin, 2001.

[21] L. Hartman and O. Hössjer. Fast kriging of large data sets with gaussian markov random fields. *Computational Statistics & Data Analysis*, 52(5):2331–2349, 2008.

[22] Diego Mendez, Miguel Labrador, and Kandethody Ramachandran. Data interpolation for participatory sensing systems. *Pervasive and Mobile Computing*, 9(1):132–148, 2013.

[23] ANSI/ASHRAE Standard 129. Measuring air change effectiveness. *Atlanta, GA: American Society of Heating, Refrigerating and Air Conditioning Engineers*, 1997.